Influence of temperature, pressure, and chemical composition on the electrical conductivity of granite

Lidong Dai, Haiying Hu, Heping Li*, Jianjun Jiang and Keshi Hui

Laboratory for High Temperature and High Pressure Study of the Earth's Interior, Institute of Geochemistry, Chinese Academy of Sciences, Guiyang, Guizhou, 550002, China

Submitted to ***American Mineralogist***

Revision 2

Revised on February 16, 2014

*Author to whom correspondence should be addressed. Electronic email: hepingli_2007@hotmail.com. Tel: 86-851-5895159. Fax: 86-851-5891749.

Abstract The electrical conductivities of granites with different chemical compositions (X_A = (Na_2O + K_2O + CaO)/SiO_2 = 0.10, 0.13, 0.14, and 0.16 in weight percent) were measured at 623–1173 K and 0.5 GPa in a multi-anvil high-pressure apparatus using a Solartron-1260 Impedance/Gain Phase analyzer within a frequency range of 10^{-1}–10^6 Hz. The conductivity of the granite sample with X_A = 0.13 was also measured at 0.5–1.5 GPa. The results indicate that pressure has a very weak influence on the electrical conductivity in the stability field of granite, whereas increases in temperature and the value of X_A produce dramatic increases in the electrical conductivity. For the granite samples with X_A = 0.16 and 0.13, the activation enthalpies are 1.0 eV above 773 K and 0.5 eV below 773 K, suggesting that impurity conduction is the dominant conduction mechanism in the lower temperature region. For the granites with X_A = 0.14 and 0.10, the activation enthalpy is 1.0 eV over the whole temperature range, suggesting that only one conduction mechanism dominates the conductivity. Based on the value of activation enthalpy (~1.0 eV) and the dependence of electrical conductivity and activation enthalpy on X_A at high temperatures, we propose that intrinsic conduction is the dominant conduction mechanism in all samples, and that K^+, Na^+, and Ca^{2+} in feldspar are the probable charge carriers controlling the conductivity. All conductivity data at high temperatures can be fitted to the general formula $\sigma = \sigma_0 X_A^{\alpha} \exp(-\frac{\Delta H_0 + \beta X_A^{\gamma}}{kT})$ where σ_0 is the pre-exponential factor; α, β, and γ are constants; ΔH_0 is the activation enthalpy at very small values of X_A; k is the Boltzmann constant; and T is the temperature. The present results suggest that the granite with various chemical compositions is unable to

account for the high conductivity anomalies under stable mid-to lower crust and southern Tibet.

Key words: electrical conductivity, granite, composition, temperature

1 Introduction

Since magnetotelluric (MT) surveys have a non-unique inverse problem and limitations in resolution and sensitivity (Bedrosian 2007), electrical conductivity data measured in the laboratory at high temperatures and pressures provide an independent approach to constraining the interpretation of MT results from the field, thus helping the geophysicist to obtain a knowledge of structure, thermal state, and composition of the interior of the Earth (Shankland and Ander 1983; Glover and Vine 1994; Yoshino 2010; Ni et al. 2011; Yang 2012; Yang et al. 2012; Pommier 2013; Selway 2013). Generally, under the defined thermodynamic conditions, the electrical conductivity of rocks is controlled mainly by the constituent minerals and their chemical compositions, although a small number of other conductive phases (e.g., water, partial melts, graphite, and other accessory conductive minerals) can also play an important role in the electrical properties of rocks (Duba et al. 1994; Ni et al. 2011; Yoshino and Noritake 2011; Yang et al. 2012). As a consequence, it is crucial to determine the relationships between the electrical conductivities of rocks and their chemical compositions before other impact factors can be clarified, because these relationships may provide significant constraints on the chemistry of the interior of the Earth.

Granite is one of the most common and widespread acid igneous rocks in the

65 Earth's crust, and large variations in its chemical composition are possible;
66 emplacement may be at depths as great as 20 km in some specific regions (Hyndman
67 1981; Guillot et al. 1995). Therefore, laboratory-measured conductivity data for
68 granites with various compositions, in combination with conductivity–depth profiles
69 derived from MT data, can provide important constraints on the composition of the
70 Earth's crust. Data on the electrical conductivity of granites under defined
71 thermodynamic conditions have been given by Noritomi and Asada (1956), Duba et al.
72 (1978), Olhoeft (1981), Parkhomenko and Bondarenko (1986), Shanov et al. (2000),
73 and Liu et al. (2001), but most of these measurements were performed at atmospheric
74 pressure using a direct current (DC) method, which means that the polarization caused
75 by the orientation of lattice defects makes the conductivity results lower than the true
76 values (Bradley et al. 1964). Furthermore, the samples used in these earlier
77 experiments were granites of a single composition. Although conductivity data were
78 calculated recently by Hu et al. (2013) for dry granites with various constituent
79 minerals, the conductivities of natural granites with different compositions have not
80 yet been measured in the laboratory at high temperatures and pressures. Consequently,
81 a systematic study of the electrical conductivity of natural granite as a function of
82 temperature, pressure, and chemical composition is well overdue.

83 For this study, we have measured the electrical conductivities of granites with
84 various chemical compositions at high temperatures and pressures by means of AC
85 complex impedance spectroscopy in a multi-anvil apparatus. For a granite sample
86 with $X_A = 0.13$, conductivity measurements were carried out at 0.5–1.5 GPa in order

to observe the effects of pressure on the electrical conductivity. On the basis of the experimental results, we discuss in detail the conduction mechanisms of granites at high temperatures and pressures. Furthermore, we have been able to determine the quantitative relationship between the electrical conductivity of dry granites and other factors such as temperature and chemical composition.

2 Experimental methods

2.1 Sample preparation

Four granite samples with different compositions were collected: two biotite granites from the Xihuashan mining area in Jiangxi province (XHS7, XHS8), a monzonitic granite from Wutai mountain in Shanxi province (SXW), and an oligoclase granite from Fuping county in Hebei province (HBP), China. These granites are fresh, leucocratic, and ash-gray to pinkish-gray in color. The granites consist predominantly of plagioclase and orthoclase (60%–70%), quartz (30%–35%), and subordinate muscovite, biotite, amphibole, and garnet (all 2%–5%). The granites are relatively fine-grained, and generally display porphyritic textures with phenocrysts of plagioclase, orthoclase, and quartz, as well as minor biotite and muscovite. The textures and fabrics of the granite samples, as seen under the polarizing microscope, are shown in Figure 1. The major element contents in each granite sample were determined with a PANalytical Axios-advance (Axios PW4400) X-Ray Fluorescence spectrometer (XRF) at the State Key Laboratory of Ore Deposit Geochemistry, Institute of Geochemistry, Chinese Academy of Sciences (CAS), Guiyang, China. The

results are given in Table 1. The analytical precision was better than 5%. The modes of the constituent minerals were determined by point counting, and those results are also given in Table 1. The analytical results allowed us to calculate the values of X_A ($(Na_2O + K_2O + CaO)/SiO_2$ in weight percent). The experimental samples were cut from blocks of the granites with a slicing machine, and polished into cylindrical shapes (Spec: 6 mm × 6 mm). The samples were then rinsed with acetone, and ethanol de-ionized water in an ultrasonic cleaning instrument. Finally, the samples were kept in an oven at 423 K overnight to remove the absorbed water until the samples were assembled for the electrical conductivity measurements.

FT–IR measurements were made on the main constituent minerals in the granite samples before and after conductivity measurements in order to determine the water contents. According to the H-related absorption bands from 3000 to 3750 cm^{-1}, the water contents in both feldspar and quartz were calculated using the equation given by Paterson (1982), and the results showed that less than ~3 H/10^6 Si and ~6 H/10^6 Si exist in the feldspar and quartz, respectively. The granite samples are therefore essentially dry during the whole experimental process.

2.2 Electrical conductivity measurement

High pressures and temperatures were generated in the YJ-3000t multi-anvil high-pressure apparatus installed in the laboratory for high temperature and high pressure study of the Earth's interior, Institute of Geochemistry, CAS. The pressures and temperatures of the apparatus were calibrated by previous work, and the details

131 can be found in Xu et al. (1994) and Dai et al. (2009). The cross-section of the sample
132 assembly for electrical conductivity measurements is shown in Figure 2, and it
133 resembles that shown in Hu et al. (2011). The pressure-transmitting medium was a
134 32.5 mm-edged cube-shaped block of pyrophyllite. To eliminate the influence of
135 pyrophyllite dehydration on the electrical conductivity measurements, the block and
136 caps made of pyrophyllite were heated at 1023 K for 5 hrs in a muffle furnace prior to
137 sample assembly. Other parts of the sample cell were kept in an oven at 423 K in
138 order to keep them dry until the sample was assembled. The heater consisted of
139 three-layers of stainless steel sheets in the shape of a tube, and it was located in the
140 pyrophyllite cube. Since crustal minerals and rocks, including the granites used in this
141 study, usually have relatively low conductivities (Bagdassarov and Delépine 2004;
142 Nover 2005; Poe et al. 2008; Fuji-ta et al. 2011), we used aluminum oxide (Al_2O_3)
143 and high-purity hexagonal boron nitride (HBN) as insulators. These insulators were
144 directly in contact with the sample in order to provide excellent insulation during the
145 impedance spectroscopy measurements. As in previous studies (Xu et al. 2000; Hu et
146 al. 2011; Dai et al. 2012), we placed a Ni shield between the Al_2O_3 and the HBN, and
147 the shield was connected to the ground in order to prevent electromagnetic
148 disturbances and to decrease the temperature gradient in the sample cell. Platinum
149 disk electrodes with a diameter of 6 mm were placed on each end of the sample, and a
150 nickel–aluminum ($Ni_{97}Al_3$) wire was connected to each electrode. The temperature
151 was measured with a Pt–$PtRh_{10}$ thermocouple with its ball head in contact with the
152 middle of the sample.

153 Impedance spectroscopic measurements were performed using the Solartron
154 1260 impedance/gain-phase analyzer with an applied voltage of 1.0 V for alternating
155 current. The measuring frequency varied from 0.1 to 10^6 Hz. The temperatures were
156 623–1173 K and the pressure 0.5 GPa. In order to elucidate the effects of pressure on
157 electrical conductivity, measurements were also made in a pressure range from 0.5 to
158 1.5 GPa for the granite sample with X_A = 0.13. The pressure was first raised to the
159 designated value at a rate of 1.0 GPa/h. For each run, once the pressure reached the
160 designated value, the temperature was increased at a rate of 20 K/min with the
161 pressure remaining constant. The complex impedance of each sample was
162 simultaneously measured at temperature intervals of 50 K during the subsequent
163 heating and cooling cycles. All complex impedance measurements were conducted in
164 two heating and cooling cycles. To obtain reproducible data, the system was stabilized
165 for several minutes at each step in temperature in order to allow the sample cell to
166 reach thermal transmission equilibrium. In most cases, the data from the first heating
167 cycle deviated very obviously from those of subsequent cycles, and they were
168 excluded from our analyses. After each run, the recovered samples were taken from
169 the sample cell and we then examined the changes in shape that had occurred. The
170 geometric distortion was very small, which means that the distortion can be neglected
171 in the data processing. During each measurement, the experimental errors in the
172 temperature and pressure gradients were no more than 10 K and 0.1 GPa, respectively.
173 The total uncertainty in the conductivity measurements, including the thermal gradient
174 in the sample cell and the impedance arc fitting, is less than 5%.

3 Results

Figure 3 shows the typical complex impedance spectra of the granite samples at 0.5 GPa in a complex plane. All of the samples exhibit similar complex impedance characteristics. As can be seen, all arcs at different temperatures are generally composed of two parts: one is an almost ideal semicircle in the high frequency domain, and the diameter of the semicircular arc is almost centered on the real axis, which represents the bulk electrical properties of the sample; the other is the additional tail that appears at the end of the first impedance arc in the lower frequency domain, and this is the usual characteristic of diffusion processes at the sample–electrode interface (Roberts and Tyburczy 1991). Therefore, only the high–frequency arc was used to determine the conductivity of the sample. According to impedance spectra theory (Nover et al. 1992; Huebner and Dillenburg 1995), the equivalent circuit of a resistor and capacitor in parallel was chosen to fit the impedance arc in order to obtain the resistance (R) of the sample. All fitting errors are no more than 2.0% of the electrical resistance. The electrical conductivity (σ) can then be calculated using the following equation

$$\sigma = \frac{1}{\rho} = \frac{l}{RS} \tag{1}$$

where l, S, and ρ are the sample length (m), cross-section area of the electrode (m^2), and resistivity of the sample (Ω·m), respectively.

Figure 4 shows the electrical conductivity of the sample with X_A = 0.14 in two heating and cooling cycles at 0.5 GPa. In the first cycle, the electrical conductivity on heating is distinctly lower than that on cooling, but the discrepancy becomes smaller

197 with increasing temperature, and the electrical conductivity values overlap at 1173 K.
198 In the second cycle, the conductivity values have good reproducibility over the whole
199 experimental temperature regime, and they are also consistent with those in the first
200 cooling cycle. The differences in the data between the first heating cycle and
201 subsequent cycles may be attributed to the disequilibrium of thermal transfer in the
202 system. Generally, the large size of the sample cell in our experiments requires a lot of
203 time to reach thermal equilibrium. As discussed by Gaillard (2004), a steady value can
204 be attained within 15 minutes at 1573 K for a dry sample, whereas for a hydrous run,
205 about 35 minutes are required to obtain a steady value. In addition, another cause of
206 the differences in data may possibly be the effects of the intra and intergranular
207 porosity on AC impedance measurements, as discussed by Roberts and Tyburczy
208 (1991). It may be the case, for example, that the granitic samples go through a
209 sintering process during the first heating cycle, and that subsequently the pores are
210 closed, resulting in reproducible measurements of electrical conductivity. For these
211 reasons, therefore, all the experimental data used to calculate electrical conductivities
212 are from the second cycle.

213 The dependence of the electrical conductivity on temperature for granite samples
214 with different compositions is shown in Figure 5. For the samples with X_A=0.14 and
215 0.10, the electrical conductivities increase with the increase of temperature, and the
216 relationship of the logarithmic electrical conductivity against the reciprocal
217 temperature is linear over the entire range of temperatures. For the samples with X_A =
218 0.16 and 0.13, the slopes change around 773 K, and become steeper towards higher

219 temperatures; this implies a change in the conduction mechanism around this
220 temperature. Accordingly, for each of these linear intervals, the temperature
221 dependency of the conductivity can be fitted by the following Arrhenius equation:

222 $$\sigma = A\exp(-\Delta H / kT) \quad (2)$$

223 where A is the pre-exponential factor (S/m), ΔH is the activation enthalpy (eV), k
224 is the Boltzmann constant (eV/K), and T is the temperature in degrees Kelvin. The
225 Arrhenius fitting parameters are obtained by separately fitting the linear segments of
226 slope, and the results are listed in Table 2. For the samples with X_A = 0.16 and 0.13,
227 the activation enthalpy is around 0.5 eV in the low-temperature region. However, for
228 all the granite samples, the activation enthalpy is around 1.0 eV in the
229 high-temperature regime.

230 The plot of electrical conductivity against temperature for the sample with X_A =
231 0.13 at pressures of 0.5–1.5 GPa (Figure 6) demonstrates that pressure has a very
232 weak effect on electrical conductivity. Consequently, because granite is stable over
233 only a very narrow pressure range in the Earth's crust (Hyndman 1981), the influence
234 of pressure on the electrical conductivity of granite can be completely ignored. This
235 means that the pressure effect on the electrical structure of the Earth's crust can be
236 excluded when constructing a laboratory-based conductivity–depth profile on the
237 basis of granite conductivity data.

238 Figure 7 illustrates electrical conductivity as a function of the ratio (X_A) of
239 alkaline and alkaline-earth oxides ($Na_2O + K_2O + CaO$) to silica (SiO_2) in granites at
240 temperatures of 823–1123 K and 0.5 GPa. It can be seen that the effect of chemical

composition on electrical conductivity is very pronounced at any one temperature. For example, the conductivity of the granite with $X_A = 0.10$ is more than one order of magnitude higher than that of the granite with $X_A = 0.16$ at each step in temperature. In addition, the granites show an almost linear increase in conductivity with increasing X_A, which implies that the electrical conductivity of the granites is controlled mainly by feldspar, because Na_2O, K_2O, and CaO are primarily present in the feldspar.

Figure 8 shows the activation enthalpy for electrical conductivity in all granite samples as a function of chemical composition (X_A), and it demonstrates the strong dependency of the activation enthalpy at high temperatures on chemical composition, so that it decreases from 1.18 to 0.93 eV as X_A increases from 0.10 to 0.16. The fitting of the activation enthalpy with variations in X_A is also shown in Figure 8. On the contrary, the activation enthalpies for two granite samples at around 0.50 eV do not exhibit any dependency on composition.

4 Discussion

4.1 Comparisons with previous studies

Our new data on the conductivity of the granites are compared in Figure 9 with data from previous studies. Olhoeft (1981) carried out measurements of the electrical conductivity of the Westerly granite as a function of pressure, free water content, and pressure, and it was found that the electrical properties of the granite are controlled dominantly by the amount of free water and the temperature, and only weakly

affected by pressure within the range of crustal pressures. This observation, about the effect of pressure, resembles our results, as shown on Figure 6. Additionally, the data of Olhoeft (1981) for dry granites are in general agreement with our data for the conductivity of granites within the same temperature range, and the activation enthalpy (1.19 eV) is also very consistent with the activation enthalpy (1.18 eV) in our sample with $X_A = 0.10$, although the chemical composition of the Westerly granite was not given by Olhoeft (1981). Abrupt changes in the conductivity of dry Westerly granite take place at a low temperature and then again at a higher temperature. The activation energy of around 0.5 eV at near room temperatures, as reported by Olhoeft (1981), is also similar to our results (about 0.5 eV) for samples with $X_A = 0.16$ and 0.13 at temperatures no greater than 823 K.

Parkhomenko and Bondarenko (1986) investigated the electrical conductivity of rocks and minerals, including granites at high temperatures and atmospheric pressure using the direct current (DC) method. Since their data for the conductivity of granites are very scattered, we chose only two sets of data to compare with ours, and Figure 9 shows that their conductivity values are much lower. This is probably a consequence of their having used the DC method, since that method typically leads to lower than true electrical conductivity values owing to the serious problem of the polarization caused by oriented lattice defects when samples are under a direct current field (Friauf 1954; Bradley 1964). In our study, AC impedance spectroscopy was utilized in order to overcome these effects of orientation polarization. Although the conductivity values of Parkhomenko and Bondarenko (1986) are much lower than ours, the activation

energies of 0.2–0.5 eV and 0.8–1.1 eV, at temperatures respectively below and above 1000 K, are almost the same as those obtained by us (0.44–0.50 eV and 0.93–1.18 eV respectively at lower and higher temperatures).

Shanov et al. (2000) measured the electrical conductivity of granite within the temperature range of 303–1273 K at ambient pressures using the bridge method with a frequency of 10^3 Hz. Liu et al. (2001) also reported the electrical conductivity of granite at 563–1133 K and 1.0 GPa using the AC impedance spectroscopy method. Our results are essentially in agreement with those of Shanov et al. (2000) in the high-temperature segment, whereas at low temperatures their data are slightly higher than ours but overlap with the results of Liu et al. (2001). The discrepancies might be due to the measurement method used by Shanov et al. (2000). Actually, the accuracy of the bridge method with a single frequency is much lower than that of AC impedance spectroscopy. In addition, the compositional differences in the granite samples might provide another reason for our conductivity values differing from those of Shanov et al. (2000), who used rocks that contained more abundant accessory minerals. As shown in Figure 9, the results of Liu et al. (2001) are slightly higher than ours, but the abrupt increase in the electrical conductivity around 773 K is also observed in our samples with X_A = 0.16 and 0.13. In addition, the activation enthalpies of 0.56 eV and 1.09 eV that is obtained by Liu et al. (2001) before and after the inflection point are extremely close to our results, as shown in Table 2. The slightly higher electrical conductivity measured by Liu et al. (2001) may be attributed to the higher contents of alkali and alkali earth in their sample which give an X_A value

307 of 0.17, compared to our samples with X_A no more than 0.16.

308 Recently, Hu et al. (2013) calculated the electrical conductivity of dry granites
309 and syenites based on the experimental conductivity data for dry alkali feldspar and
310 quartz at 1.0 GPa. Here we chose the data of alkali-feldspar granite to compare with
311 ours, because this composition (that of 70% $Or_{40}Ab_{60}$ and 30% quartz) is very close to
312 ours. As shown in Figure 9, the data from Hu et al. (2013) are in good agreement with
313 ours within the same temperature range. The activation energy (0.91 eV) for this
314 alkali-feldspar granite is also very close to the range of our results (0.93–1.27 eV) for
315 the high-temperature regime.

316

317 **4.2 Conduction mechanism**

318 Since the Arrhenius plot demonstrates linear slopes for the samples with X_A =
319 0.14 and 0.10, as shown in Figure 5, only one conduction mechanism exists over the
320 experimental temperature range. However, for the samples with X_A = 0.16 and 0.13,
321 the slope changes at 773 K, implying the presence of two different conduction
322 mechanisms at low and high temperatures, characterized by different activation
323 enthalpies. For the samples with X_A = 0.16 and 0.13, we propose that the conduction
324 mechanism at low temperatures is extrinsic (impurity dominated) conduction due to
325 the low activation enthalpy (~0.5 eV), whereas for all samples at higher temperatures
326 intrinsic conduction is suggested to be the dominant mechanism owing to the
327 relatively high activation enthalpy (~1.0 eV), as observed in many previous studies of
328 the electrical conductivity of rocks (Alvarez et al. 1978; Olhoeft 1981; Parkhomenko

329 and Bondarenko 1986; Liu et al. 2001). Generally, the activation enthalpy for extrinsic
330 conductivity is much lower than for intrinsic conductivity since the energy necessary
331 for the migration of the pre-existing lattice defects is small according to the standpoint
332 of the ionic conduction theory of crystals (Lasaga 1981; Samara 1984). In our study,
333 the impurity conduction at low temperatures for samples with X_A = 0.16 and 0.13 may
334 be attributed to a slight weathering or alteration of samples during their long existence
335 in the Earth's crust. Additionally, the values for loss on ignition (L.O.I.) shown in
336 Table 1 are more than 0.20 for each granite sample, which means that small amounts
337 of impurity such as carbon dioxide and absorbed water may be present along
338 microcracks or microfractures in the granites, ultimately resulting in impurity
339 conduction at low temperatures.

340 For the samples with X_A = 0.14 and 0.10, the impurity conduction has not been
341 observed over the entire range of experimental temperatures. However, the activation
342 enthalpies in the higher-temperature regime vary in the range from 0.93 to 1.18 eV for
343 all granites, suggesting a dominant intrinsic conduction. Our results have
344 demonstrated the strong dependency of electrical conductivity and activation enthalpy
345 on X_A for all granite samples at high temperatures. A similar study concerning
346 electrical conductivity as a function of K^+ and Na^+ in alkali feldspar has recently been
347 demonstrated by Hu et al. (2013), who found that the electrical conductivity of alkali
348 feldspar dramatically depends on the concentration of alkali ions; the activation
349 enthalpy is about 1.0 eV, which indicates that K^+ and Na^+ are the main
350 charge-transporting carriers in the feldspar. Our study has shown the same tendency

and a similar activation enthalpy (0.93–1.18 eV) in the granites, which suggests that the bulk conductivity can be mainly attributed to K^+, Na^+, and Ca^{2+} in feldspar due to the presence of large amounts of interconnected feldspar in the granites.

The data for the electrical conductivity of igneous rocks, given by Alvarez et al. (1978), also show an increase in conductivities with the increase in the total content of $Na_2O + K_2O + CaO$, and the activation energies strongly depend on X_A. In addition, during heating the activation energies for dacite and rhyolite samples at 573–873 K are 1.12 eV and 1.28 eV, respectively, which generally agree with those determined by us (0.93–1.18 eV). Consequently, the similar results for electrical conductivity and activation enthalpy at the high-temperature region in our study and that of Alvarez et al. (1978) further support the proposition that intrinsic conduction is the dominant conduction mechanism, and that K^+, Na^+, and Ca^{2+} are the most important charge carriers owing to their higher concentrations and mobilities when compared with other ions in granites.

According to ionic conduction theory (Samara 1984), the concentration of charge carriers increase with increasing temperature because the concentration and motions of intrinsic defects are activated processes. On the contrary, for extrinsic conduction the change in charge carrier concentration with temperature is negligible. Accordingly, the measured activation energy is simply associated with the motion of the mobile species. Consequently, the activation enthalpy for intrinsic conduction is much higher than that for extrinsic conduction. In our results, the activation enthalpy at high temperatures is about twice that is correspondent at low temperatures, which further

indicates that it is the intrinsic defects, rather than the impurities, that contribute to the bulk conductivity at high temperatures. Nevertheless, other candidates for the role of charge carrier such as Fe^{2+}, Fe^{3+}, Mg^{2+}, and Mn^{2+} are not likely to play an important role because these ions are in very low concentrations, and mainly present in garnet, hornblende, or other accessory minerals that occur as isolated grains rather than as an interconnected network like the feldspars in granite. Based on the analysis above, K^{+}, Na^{+}, and Ca^{2+} in feldspar are the most likely candidates for dominating the conduction in dry granite in high-temperature regimes.

4.3 Effects of temperature and composition on intrinsic conduction

Since the electrical conductivity of rocks is quite sensitive to the constituent minerals as well as temperature, pressure, humidity, porosity, minor impurities, texture, fluid, and oxygen fugacity, it is much more difficult to construct the conductivity model for a rock as a function of these factors, when compared with a mineral. Although many previous researchers have successfully established the relationship between some factors (e.g. temperature, pressure, oxygen fugacity, chemical composition and water) and the electrical conductivity of minerals such as ringwoodite (Yoshino and Katsura 2009), wadsleyite (Dai and Karato 2009a), ferropericlase (Yoshino et al. 2011), olivine (Hirsch et al. 1993; Dai et al. 2008, 2010; Yoshino et al. 2012), enstatite (Zhang et al. 2012), and garnet (Tolland 1973; Romano et al. 2006; Dai and Karato 2009b; Dai et al. 2012, 2013), it is insufficient to use the data of minerals to construct a conductivity-depth profile when attempting to

395 determine the composition and structure of the Earth, because rocks rather than
396 minerals are the major constituent materials in the Earth's crust and mantle. From
397 Figure 7, it is clear that temperatures and chemical compositions have strong
398 influences on the electrical conductivity of granites in the high-temperature regime.
399 Meanwhile, the activation enthalpies decrease with an increase in X_A, as shown in
400 Figure 8, and the relationship between the activation enthalpy (ΔH) and the value of
401 X_A can therefore be approximated by the following equation for the intrinsic
402 conduction region in a similar way to previous work with Fe-rich olivine and its
403 high-pressure polymorphs (Yoshino et al. 2012):

404 $$\Delta H = \Delta H_0 + \beta X_A^{\gamma} \quad (3)$$

405 where X_A is the weight percent ratio of $Na_2O + K_2O + CaO$ to SiO_2 in the granites,
406 ΔH and ΔH_0 are the activation enthalpies at the specific X_A and at a very small X_A,
407 respectively, and β and γ are constants that account for the geometrical factors.
408 As shown in Figure 8, the relationship between activation enthalpy and X_A is well
409 fitted by Eq. (3), and the relevant parameters are presented in Table 3.

410 Taking into account the effects of the concentration of charge carriers on the
411 pre-exponential factor, the electrical conductivities of granites with different chemical
412 compositions can be expressed as follows

413 $$\sigma = \sigma_0 X_A^{\alpha} \exp(-\frac{\Delta H_0 + \beta X_A^{\gamma}}{kT}) \quad (4)$$

414 where σ_0 is the pre-exponential factor in the intrinsic conduction regime, and α is a
415 constant. According to Eq. (4), our high-temperature data are fitted by using global
416 least-squares fitting, and the fitting parameters are summarized in Table 3. Using the

417 fitting parameters in Table 3 and Eq. (4), the electrical conductivities of granites for
418 the high-temperature region can be calculated, and the results are given in Figure 5.
419 As illustrated in Figure 5, the calculated values of conductivity are in good agreement
420 with the experimental values in the high-temperature region, except that the value for
421 the sample with $X_A = 0.10$ is about 0.2 log unit lower than the measured value at high
422 temperatures, but the discrepancy becomes smaller as temperatures decrease. The
423 discrepancy may be attributed to the discontinuous variations of the measured
424 activation enthalpy with X_A, especially for the sample with $X_A = 0.10$ where the
425 activation enthalpy abruptly reaches up to 1.18 eV, as shown in Table 2. The effects of
426 pressure are not included in Eq. (4). This is because our results have shown that
427 pressure has only a very weak effect on the electrical conductivity of granite, as
428 shown in Figure 6, and granite is stable over only a very narrow range of pressures in
429 the Earth's crust.
430

431 **5 Geophysical implications**

432 Granite, as the most common and widespread rock in the continental crust, is
433 likely to account for the high-conductivity anomalies observed in the crust, especially
434 in tectonically-active regions. Therefore, based on two geothermal gradient models
435 with average heat flow value of 60 mW/m^2 and 90 mW/m^2 for the stable continental
436 crust and Tibet plateau (Pollack 1993; Hu et al. 2000), respectively, two sets of
437 laboratory-based conductivity-depth profiles are constructed by using the parameters
438 determined by equation (4) in high temperature regions and extrapolating

impurity-related conductivity data to shallower region. Accordingly, the two sets of profiles are compared with the anomalous high conductivity zone under the stable mid-to lower continental crust at the depth of 20-30 km with conductivity of ~10^{-2}-10^{-1} S/m (Marquis and Hyndman, 1992, Glover and Vine, 1994) and the high electrical conductivities in the middle crust of southern Tibet at depths of 10-20 km with conductivity of no less than 10^{-1} S/m (Chen et al. 1996; Li et al. 2003; Wei et al. 2001, 2010), respectively. The results are shown in Fig. 10.

The profiles clearly show that the electrical conductivities of granite with various chemical compositions at least by 3 log units lower than that of anomalous high-conductivity layer beneath the stable continental crust and southern Tibet, although the chemical composition has a considerable effect on the conductivity structure of the continental crust showed in Fig. 10. Therefore, the granite with various chemical compositions cannot account for the observed high-conductivity anomalies that are inferred from magnetotelluric data. However, the upper crust overlying the high conductivity zone usually has low electrical conductivity, which is typical of different constituent rocks, and the layer markedly shows lateral variation in electrical conductivity (Bai et al. 2010; Wei et al. 2010). Consequently, the present conductivity-depth profile constructed by granites with various chemical compositions may provide important constraints on the interpretation of field magnetotelluric results for definition of the composition of the Earth's interior as a function of depth.

Acknowledgments

This research was supported financially by the “135” Program of the Institute of Geochemistry, Chinese Academy of Sciences, and the NSF of China (41304068 and 41174079).

References

[1] Alvarez, R., Reynoso, J.P., Alvarez, L.J., and Martinez, M.L. (1978) Electrical conductivity of igneous rocks: composition and temperature relations. Bull Volcanol, 41, 317–327.

[2] Bagdassarov, N.S., and Delépine, N. (2004) α–β inversion in quartz from low frequency electrical impedance spectroscopy. Journal of Physics and Chemistry of Solids, 65, 1517–1526.

[3] Bai, D., Unsworth, M.J., Meju, M.A., Ma, X., Teng, J., Kong, X., Sun, Y., Sun, J., Wang, L., Jiang, C., Zhao, C., Xiao, P., and Liu, M. (2010) Crustal deformation of the eastern Tibetan plateau revealed by magnetotelluric imaging. Nature Geoscience, 3, 358–362.

[4] Bedrosian, P.A. (2007) MT+, integrating magnetotellurics to determine earth structure, physical state, and processes. Surveys in Geophysics, 28, 121–167.

[5] Bradley, R., Jamil, A., and Munro, D.C. (1964) The electrical conductivity of olivine at high temperatures and pressures. Geochimica et Cosmochimica Acta, 28, 1669–1678.

[6] Chen, L., Booker, J.R., Jones, A.G., Wu, N., Unsworth, M.J., Wei, W., and Tan, H. (1996) Electrically conductive crust in southern Tibet from INDEPTH magnetotelluric surveying. Science, 274, 1694–1696.

[7] Dai, L., and Karato, S. (2009a) Electrical conductivity of wadsleyite at high temperatures and high pressures. Earth and Planetary Science Letters, 287, 277–283.

[8] Dai, L., and Karato, S. (2009b) Electrical conductivity of pyrope-rich garnet at

high temperature and high pressure. Physics of the Earth and Planetary Interiors, 176, 83–88.

[9] Dai, L., Li, H., Hu, H., and Shan, S. (2008) Experimental study of grain boundary electrical conductivities of dry synthetic peridotite under high-temperature, high-pressure, and different oxygen fugacity conditions. Journal of Geophysical Research-Solid Earth, 113, B12211, doi:10.1029/2008JB005820.

[10] Dai, L., Li, H., Hu, H., and Shan, S. (2009) Novel technique to control oxygen fugacity during high-pressure measurements of grain boundary conductivities of rocks. Review of Scientific Instruments, 80, 033903, doi:10.1063/1.3097882.

[11] Dai, L., Li, H., Li, C., Hu, H., and Shan, S. (2010) The Electrical conductivity of dry polycrystalline olivine compacts at high temperatures and pressures. Mineralogical Magazine, 74, 849–857.

[12] Dai, L., Li, H., Hu, H., Shan, S., Jiang, J., and Hui, K. (2012) The effect of chemical composition and oxygen fugacity on the electrical conductivity of dry and hydrous garnet at high temperatures and pressures. Contributions to Mineralogy and Petrology, 163, 689–700.

[13] Dai L., Li, H., Hu, H., Jiang, J., Hui, K., and Shan, S. (2013) Electrical conductivity of $Alm_{82}Py_{15}Grs_3$ almandine-rich garnet determined by impedance spectroscopy at high temperatures and high pressures. Tectonophysics, 2013, 608, 1086–1093.

[14] Duba, A., Piwinskii, A.J., Santor, M., and Weed, H.C. (1978) The electrical conductivity of sandstone, limestone and granite. Geophysical Journal of the

511 Royal Astronomical Society, 53, 583–597.
512 [15] Duba, A., Heikamp, S., Meurer, W., Nover, G., and Will, G. (1994) Evidence from
513 borehole samples for the role of accessory minerals in lower-crustal conductivity.
514 Nature, 367, 59–61.
515 [16] Friauf, R.J. (1954) Polarization effects in the ionic conductivity of silver bromide.
516 The Journal of Chemical Physics, 22, 1329–1338.
517 [17] Fuji-ta, K., Katsura, T., Ichiki, M., Matsuzaki, T., and Kobayashi, T. (2011)
518 Variations in electrical conductivity of rocks above metamorphic conditions.
519 Tectonophysics, 504, 116–121.
520 [18] Gaillard, F. (2004) Laboratory measurements of electrical conductivity of
521 hydrous and dry silicic melts under pressure. Earth and Planetary Science Letters,
522 218, 215–228.
523 [19] Glover, P., and Vine, F. (1994) Electrical conductivity of the continental crust.
524 Geophysical Research Letters, 21, 2357–2360.
525 [20] Guillot, S., Le Fort, P., Pêcher, A., Roy Barman, M., and Aprahamian, J. (1995)
526 Contact metamorphism and depth of emplacement of the Manaslu granite (central
527 Nepal). Implications for Himalayan orogenesis. Tectonophysics, 241, 99–119.
528 [21] Hirsch, L.M., Shankland, T.J., and Duba, A.G. (1993) Electrical conduction and
529 polaron mobility in Fe-bearing olivine. Geophysical Journal International, 114,
530 36–44.
531 [22] Hu, H., Li, H., Dai, L., Shan, S., and Zhu, C. (2011) Electrical conductivity of
532 albite at high temperatures and high pressures. American Mineralogist, 96,

1821–1827.

[23] Hu, H., Li, H., Dai, L., Shan, S., and Zhu, C. (2013) Electrical conductivity of alkali feldspar solid solutions at high temperatures and high pressures. Physics and Chemistry of Minerals, 40, 51–62.

[24] Hu, S., He, L., and Wang, J. (2000) Heat flow in the continental area of China: a new data set. Earth and Planetary Science Letters, 179, 407–419.

[25] Huebner, J.S., and Dillenburg, R.G. (1995) Impedance spectra of hot, dry silicate minerals and rock: qualitative interpretation of spectra. American Mineralogist, 80, 46–64.

[26] Hyndman, D. (1981) Controls on source and depth of emplacement of granitic magma. Geology, 9, 244–249.

[27] Lasaga, A. C. (1981) The atomistic basis of kinetics: defects in minerals. Reviews in Mineralogy and Geochemistry, 8, 261–319.

[28] Li, S., Unsworth, M.J., Booker, J.R., Wei, W., Tan, H., and Jones, A.G. (2003) Partial melt or aqueous fluid in the mid-crust of southern Tibet? Constraints from INDEPTH magnetotelluric data. Geophysical Journal International 153, 289–304.

[29] Liu, J., Bai, W., Kong, X., and Zhu, M. (2001) Electrical conductivity of granite, basalt and pyroxene peridotite under high temperature–high pressure conditions. Chinese Journal of Geophysics, 44, 528–533.

[30] Marquis, G., and Hyndman, R.D. (1992) Geophysical support for aqueous fluids in the deep crust: seismic and electrical relationships. Geophysical Journal International, 110, 91–105.

[31] Ni, H., Keppler, H., and Behrens, H. (2011) Electrical conductivity of hydrous

basaltic melts: implications for partial melting in the upper mantle. Contributions to Mineralogy and Petrology, 162, 637–650.

[32] Noritomi, K., and Asada, A. (1956) Studies on the electrical conductivity of a few samples of granite and andesite. Science Reports Tohoku Univ., Fifth Ser. 7, 201–207.

[33] Nover, G., Will, G., and Waitz, R. (1992) Pressure induced phase transition in Mg_2GeO_4 as determined by frequency dependent complex electrical resistivity measurements. Physics and Chemistry of Minerals, 19, 133–139.

[34] Nover, G. (2005) Electrical properties of crustal and mantle rocks—a review of laboratory measurements and their explanation. Surveys in Geophysics, 26, 593–651.

[35] Olhoeft, G. (1981) Electrical properties of granite with implications for the lower crust. Journal of Geophysical Research, 86, 931–936.

[36] Parkhomenko, E., and Bondarenko, A. (1986) Electrical conductivity of rocks at high pressures and temperatures. NASA, Washington, D.C. pp 65–75.

[37] Paterson, M.S. (1982) The determination of hydroxyl by infrared absorption in quartz, silicate glasses and similar materials. Bulletin de Minéralogie, 105, 20–29.

[38] Poe, B.T., Romano, C., Varchi, V., Misiti, V., and Scarlato, P. (2008) Electrical conductivity of a phonotephrite from Mt. Vesuvius: the importance of chemical composition on the electrical conductivity of silicate melts. Chemical Geology, 256, 192–201.

[39] Pollack, H.N., Hurter, S.J., and Johnson, J.R. (1993) Heat flow from the Earth's

578 interior: analysis of the global data set. Reviews of Geophysics, 31, 267–280.
579 [40] Pommier, A. (2014) Interpretation of magnetotelluric results using laboratory
580 measurements. Surveys in Geophysics, 35, 41–84.
581 [41] Roberts, J.J. and Tyburczy, J. A. (1991) Frequency dependent electrical properties
582 of polycrystalline olivine compacts. Journal of Geophysical Research, 96(B10),
583 16205–16222.
584 [42] Romano, C., Poe, B.T., Kreidie, N., and McCammon, C.A. (2006) Electrical
585 conductivities of pyrope–almandine garnets up to 19 GPa and 1700 °C. American
586 Mineralogist, 91, 1371–1377.
587 [43] Samara, G.A. (1984) High-pressure studies of ionic conductivity in solids. Solid
588 State Physics, 38, 1–80.
589 [44] Selway, K. (2014) On the causes of electrical conductivity anomalies in
590 tectonically stable lithosphere. Surveys in Geophysics, 35, 219–257.
591 [45] Shankland, T.J., and Ander, M.E. (1983) Electrical conductivity, temperatures,
592 and fluids in the lower crust. Journal of Geophysical Research, 88, 9475–9484.
593 [46] Shanov, S., Yanev, Y., and Lastovickova, M. (2000) Temperature dependence of
594 the electrical conductivity of granite and quartz–monzonite from south Bulgaria:
595 geodynamic inferences. Journal of the Balkan Geophysical Society, 3, 13–19.
596 [47] Tolland, H. (1973) Mantle conductivity and electrical properties of garnet, mica
597 and amphibole. Nature, 241, 35–36.
598 [48] Wei, W., Unsworth, M., Jones, A., Booker, J., Tan, H., Nelson, D., Chen, L., Li, S.,
599 Solon, K., Bedrosian, P., Jin, S., Deng, M., Ledo, J., Kay, D., and Roberts, B.

(2001) Detection of widespread fluids in the Tibetan crust by magnetotelluric studies. Science, 292, 716–719.

[49] Wei, W., Jin, S., Ye, G., Deng, M., Jing, J., Unsworth, M., and Jones, A.G. (2010) Conductivity structure and rheological property of lithosphere in southern Tibet inferred from super-broadband magnetotelluric sounding. Science China Earth Sciences, 53, 189–202.

[50] Xu, J., Zhang, Y., Hou, W., Xu, H., Guo, J., Wang, Z., Zhao, H., Wang, R., Huang, E., and Xie, H. (1994) Measurements of ultrasonic wave velocities at high temperature and high pressure for window glass, pyrophyllite, and kimberlite up to 1400° C and 5.5 GPa. High Temperature–High Pressure, 26, 375–384.

[51] Xu, Y., Shankland, T.J., and Duba, A.G. (2000) Pressure effect on electrical conductivity of mantle olivine. Physics of the Earth and Planetary Interiors, 118, 149–161.

[52] Yang, X. (2012) Orientation-related electrical conductivity of hydrous olivine, clinopyroxene and plagioclase and implications for the structure of the lower continental crust and uppermost mantle. Earth and Planetary Science Letters, 317–318, 241–250.

[53] Yang, X., Keppler, H., McCammon, C., and Ni, H. (2012) Electrical conductivity of orthopyroxene and plagioclase in the lower crust. Contributions to Mineralogy and Petrology, 163, 33–48.

[54] Yoshino, T., and Katsura, T. (2009) Effect of iron content on electrical conductivity of ringwoodite, with implications for electrical structure in the

622 transition zone. Physics of the Earth and Planetary Interiors, 174, 3–9.
623 [55] Yoshino, T. (2010) Laboratory electrical conductivity measurement of mantle
624 minerals. Surveys in Geophysics, 31, 163–206.
625 [56] Yoshino, T., and Noritake, F. (2011) Unstable graphite films on grain boundaries
626 in crustal rocks. Earth and Planetary Science Letters, 306, 186–192.
627 [57] Yoshino, T., Ito, E., Katsura, T., Yamazaki, D., Shan, S., Guo, X., Nishi, M., Higo,
628 Y., and Funakoshi, K. (2011) Effect of iron content on electrical conductivity of
629 ferropericlase with implications for the spin transition pressure. Journal of
630 Geophysical Research, 116, B04202, doi:10.1029/2010JB007801.
631 [58] Yoshino, T., Shimojuku, A., Shan, S., Guo, X., Yamazaki, D., Ito, E., Higo, Y.,
632 and Funakoshi, K. (2012) Effect of temperature, pressure and iron content on the
633 electrical conductivity of olivine and its high-pressure polymorphs. Journal of
634 Geophysical Research, 117, B08205, doi:10.1029/2011JB008774.
635 [59] Zhang, B., Yoshino, T., Wu, X., Matsuzaki, T., Shan, S., and Katsura, T. (2012)
636 Electrical conductivity of enstatite as a function of water content: implications for
637 the electrical structure in the upper mantle. Earth and Planetary Science Letters,
638 357, 11–20.
639

Figure captions

Figure 1. Photomicrographs of four granite samples under the polarizing microscope. Pl, plagioclase; Qtz, quartz; Or, orthoclase; Bi, biotite.

Figure 2. Schematic cross-section of the sample assembly for electrical conductivity measurements in the multi-anvil high-pressure apparatus.

Figure 3. Representative complex spectra of granite samples at 673–1173 K and 0.5 GPa in the frequency range from 0.1 to 10^6 Hz. Z' and Z'' are the real and imaginary parts of the complex impedance, respectively.

Figure 4. Electrical conductivity of the sample with X_A = 0.14 in two heating and cooling cycles at 0.5 GPa. The data from the first heating cycle deviate from those in the subsequent cycles owing to the disequilibrium of thermal transfer in the system.

Figure 5. Electrical conductivities of dry granites with different chemical compositions plotted as a function of temperature at 0.5 GPa. The black dashed lines represent the Arrhenius fitting results, the colored solid lines indicate the fitting results obtained using Eq. (4) in the high-temperature region, and the legends near the lines represent the sample compositions, given as X_A.

Figure 6. Logarithm of electrical conductivity of the sample with X_A = 0.13 versus

662 reciprocal temperature at pressures of 0.5–1.5 GPa.

663

664 **Figure 7.** Electrical conductivity of dry granites in the intrinsic conduction region
665 plotted as a function of X_A ($(Na_2O + K_2O + CaO)/SiO_2$) at 0.5 GPa.

666

667 **Figure 8.** Activation enthalpies for the electrical conductivity of dry granites in the
668 intrinsic conduction region and the impurity conduction region plotted as a function of
669 X_A. The red solid line shows the fitting results using Eq. (3).

670

671 **Figure 9.** Comparison of electrical conductivities of dry granites measured in this
672 study with previous data. Symbols show our results for the electrical conductivities of
673 dry granites. The blue solid line denotes the data for dry Westerly granite (from
674 Olhoeft 1981). The purple lines denote the electrical conductivities of granites
675 measured by Parkhomenko and Bondarenko (1986) with the DC method at ambient
676 pressure. The red line denotes the data for granite at ambient pressure using the bridge
677 method (from Shanov et al. 2000). The dark yellow line denotes the data for granite at
678 1.0 GPa using the AC impedance spectroscopy method (Liu et al. 2001). The green
679 line denotes the theoretical calculated result for a dry granite with 70% alkali feldspar
680 and 30% quartz at 1.0 GPa (Hu et al. 2013).

681

682 **Figure 10.** Two sets of laboratory-based conductivity-depth profile as a function of
683 chemical composition (X_A=0.12-0.16) compared with anomalous high conductivity

684 zones (HCZ) under the stable mid-lower continental crust and southern Tibet,
685 respectively, observed by field geophysical method. The dark orange lines and black
686 lines represent the laboratory-based conductivity-depth profiles based on 90 mW/m^2
687 heat flow value for Tibet plateau and 60 mW/m^2 heat flow value for the stable
688 continental crust, respectively. The dark orange region denotes the high conductivity
689 anomalies beneath southern Tibet at a depth of 10 to 20 km (Chen et al. 1996; Wei et
690 al. 2001). The gray region shows that the HCZ in the stable mid-to lower continental
691 crust at depths of 20–30 km (Glover and Vine, 1994).

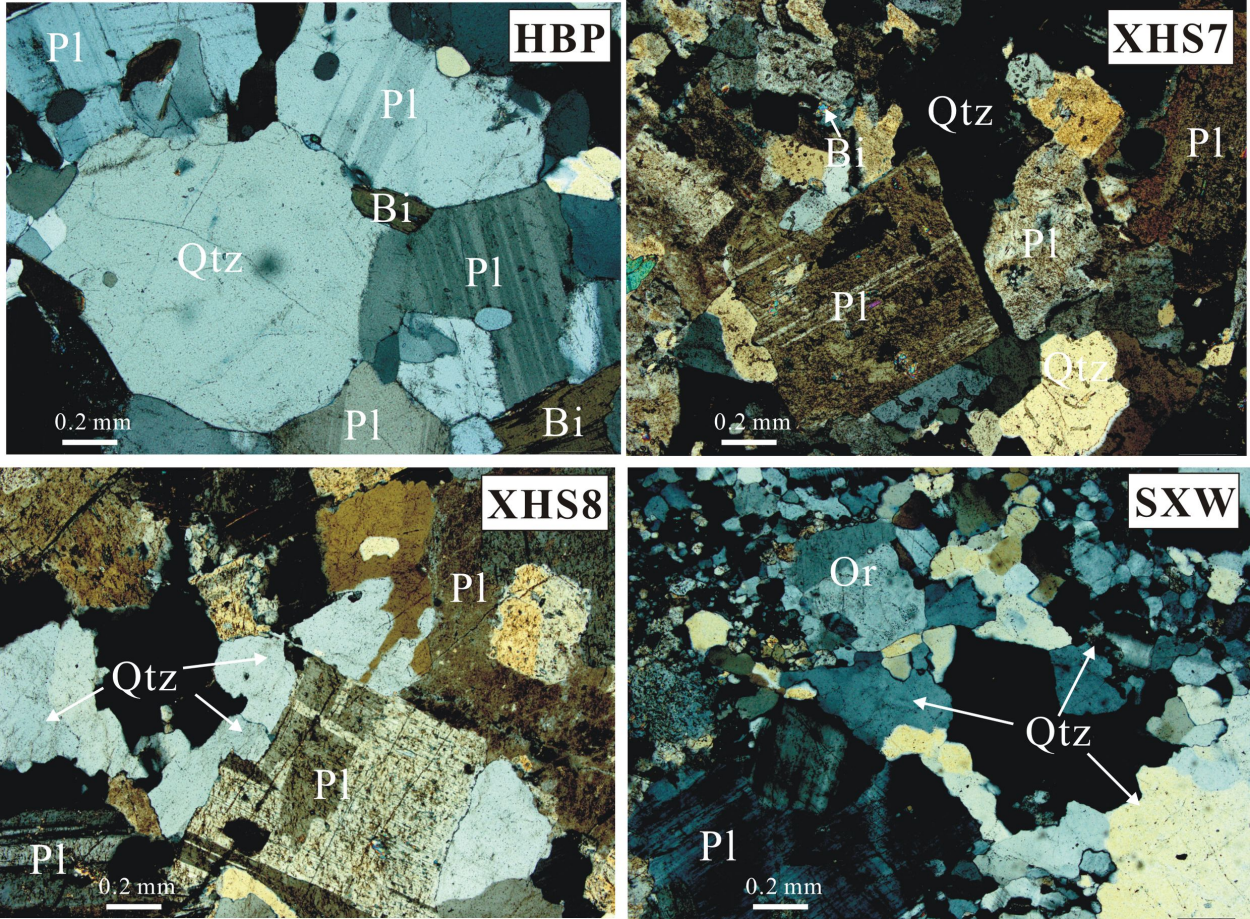
HBP
Pl
Pl
Bi
Qtz
Pl
Pl
Bi
0.2 mm
XHS7
Qtz
Bi
Pl
Pl
Pl
Qtz
0.2 mm
XHS8
Pl
Qtz
Pl
Pl
0.2 mm
SXW
Or
Qtz
Pl
0.2 mm

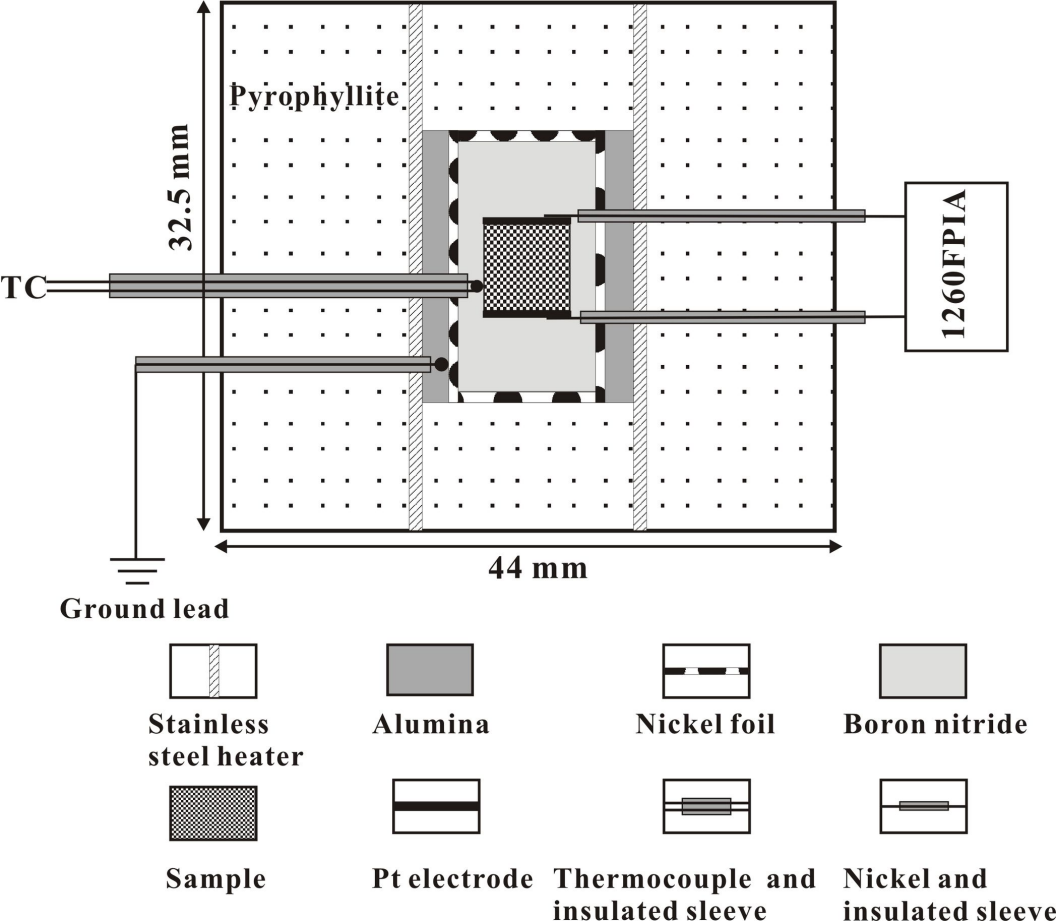
Pyrophyllite
32.5 mm
TC
1260FPIA
44 mm
Ground lead
Stainless steel heater
Alumina
Nickel foil
Boron nitride
Sample
Pt electrode
Thermocouple and insulated sleeve
Nickel and insulated sleeve

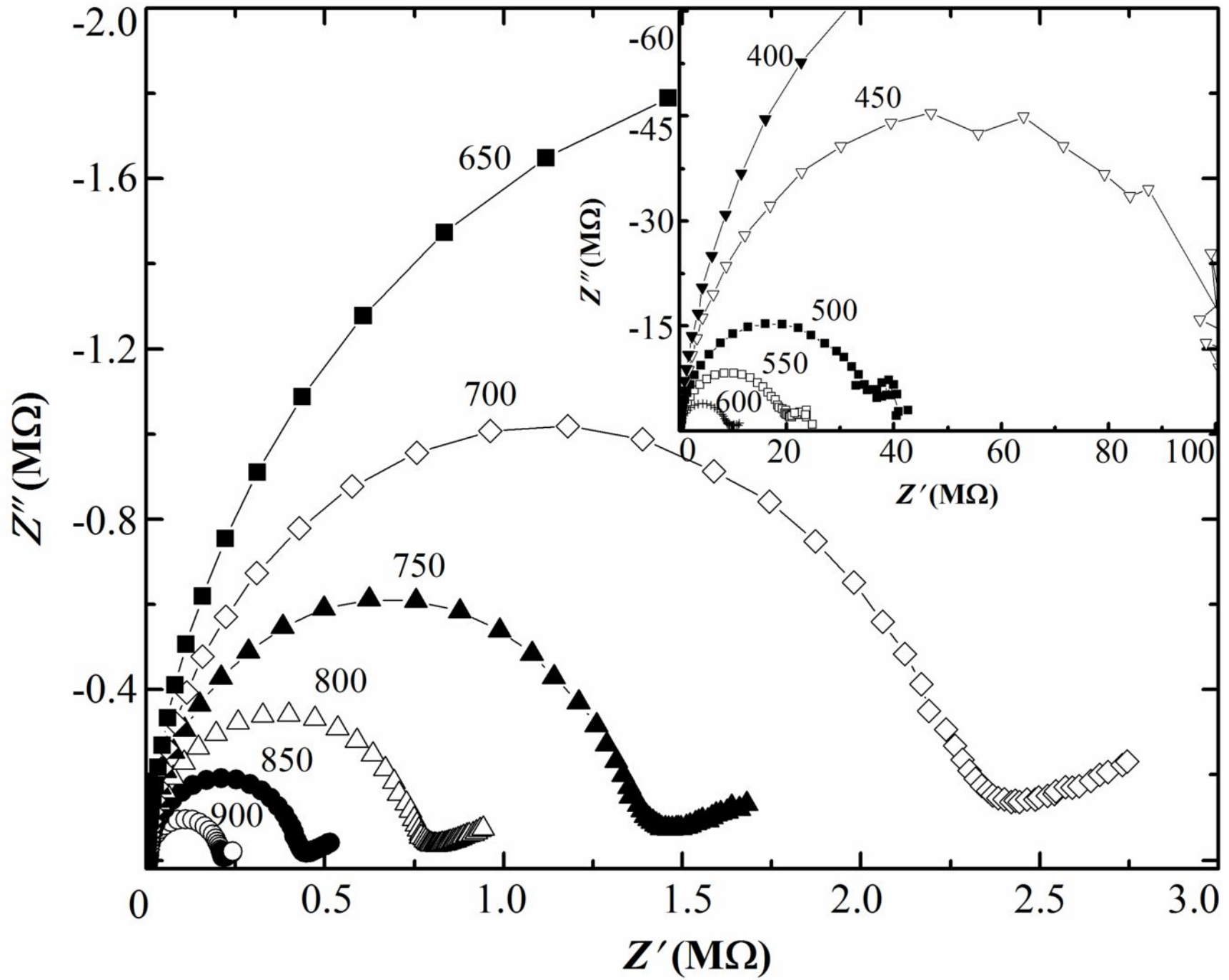
-2.0
-1.6
-1.2
-0.8
-0.4
0
0.5
1.0
1.5
2.0
2.5
3.0
Z″(MΩ)
Z′(MΩ)
650
700
750
800
850
900
-60
-45
-30
-15
0
20
40
60
80
100
400
450
500
550
600

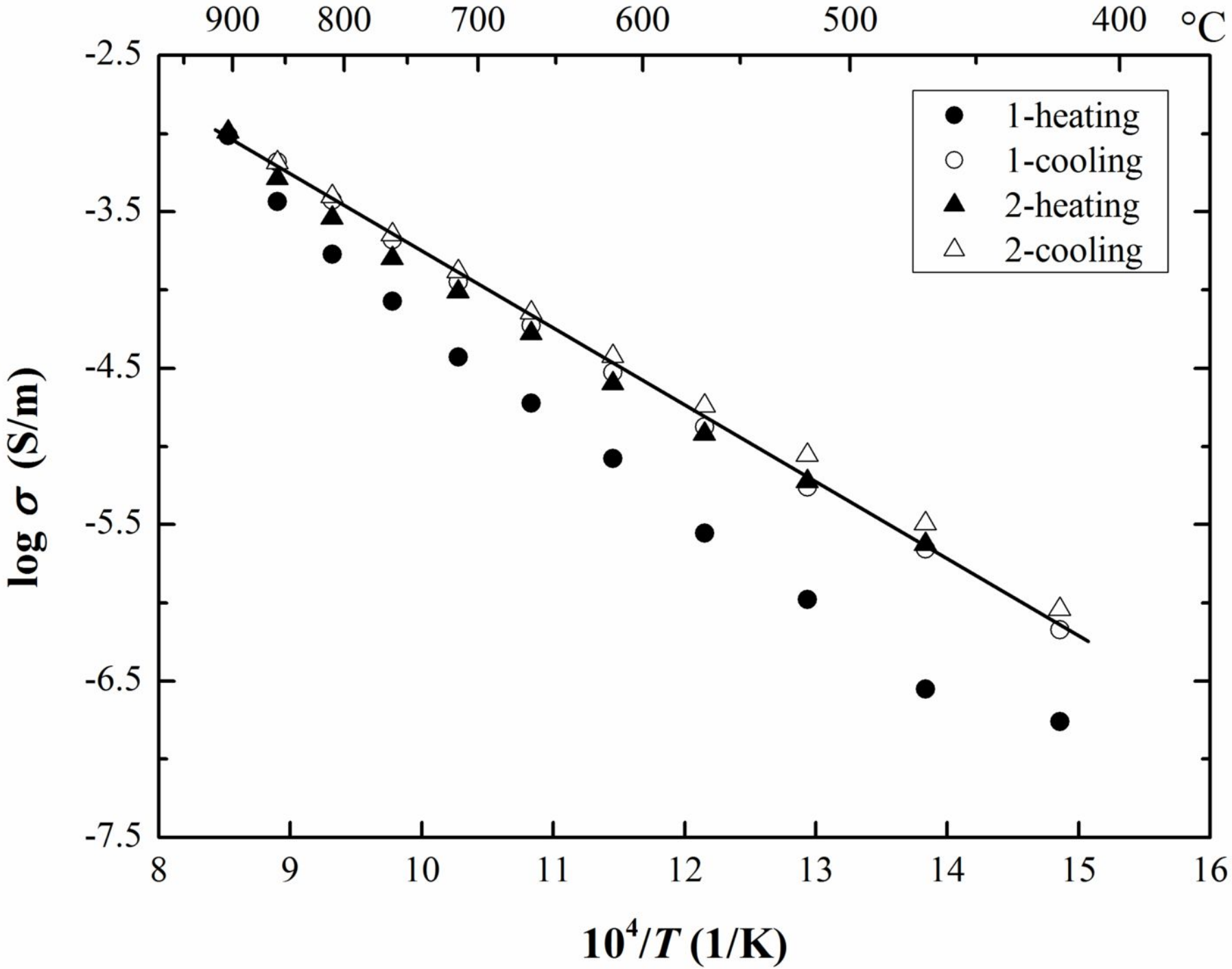
900
800
700
600
500
400
°C
-2.5
-3.5
-4.5
-5.5
-6.5
-7.5
log σ (S/m)
8
9
10
11
12
13
14
15
16
10^4/T (1/K)
1-heating
1-cooling
2-heating
2-cooling

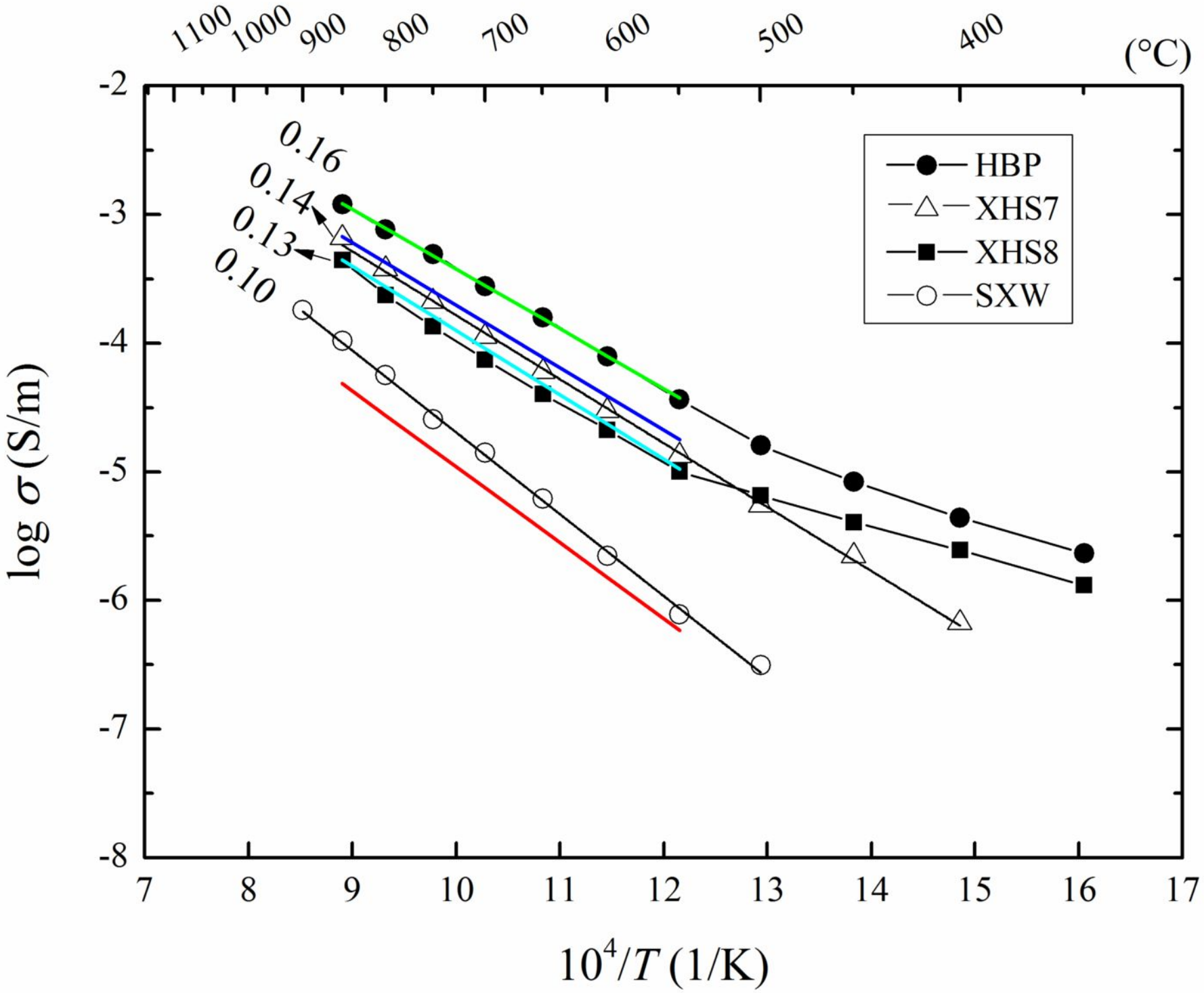
1100
1000
900
800
700
600
500
400
(°C)
-2
-3
-4
-5
-6
-7
-8
log σ (S/m)
7
8
9
10
11
12
13
14
15
16
17
10^4/T (1/K)
0.16
0.14
0.13
0.10
HBP
XHS7
XHS8
SXW

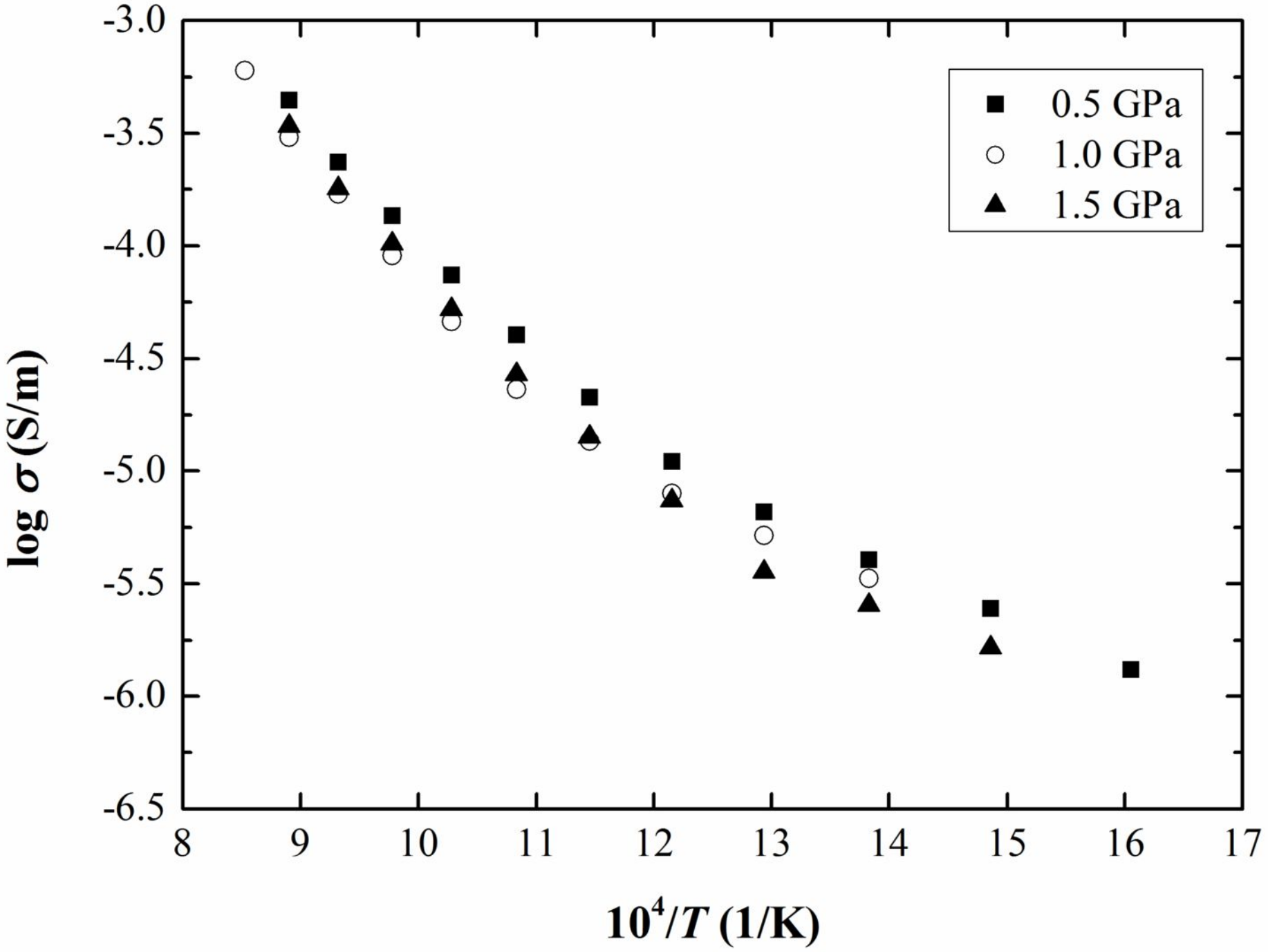
-3.0
-3.5
-4.0
-4.5
-5.0
-5.5
-6.0
-6.5
log σ (S/m)
8
9
10
11
12
13
14
15
16
17
10^4/T (1/K)
0.5 GPa
1.0 GPa
1.5 GPa

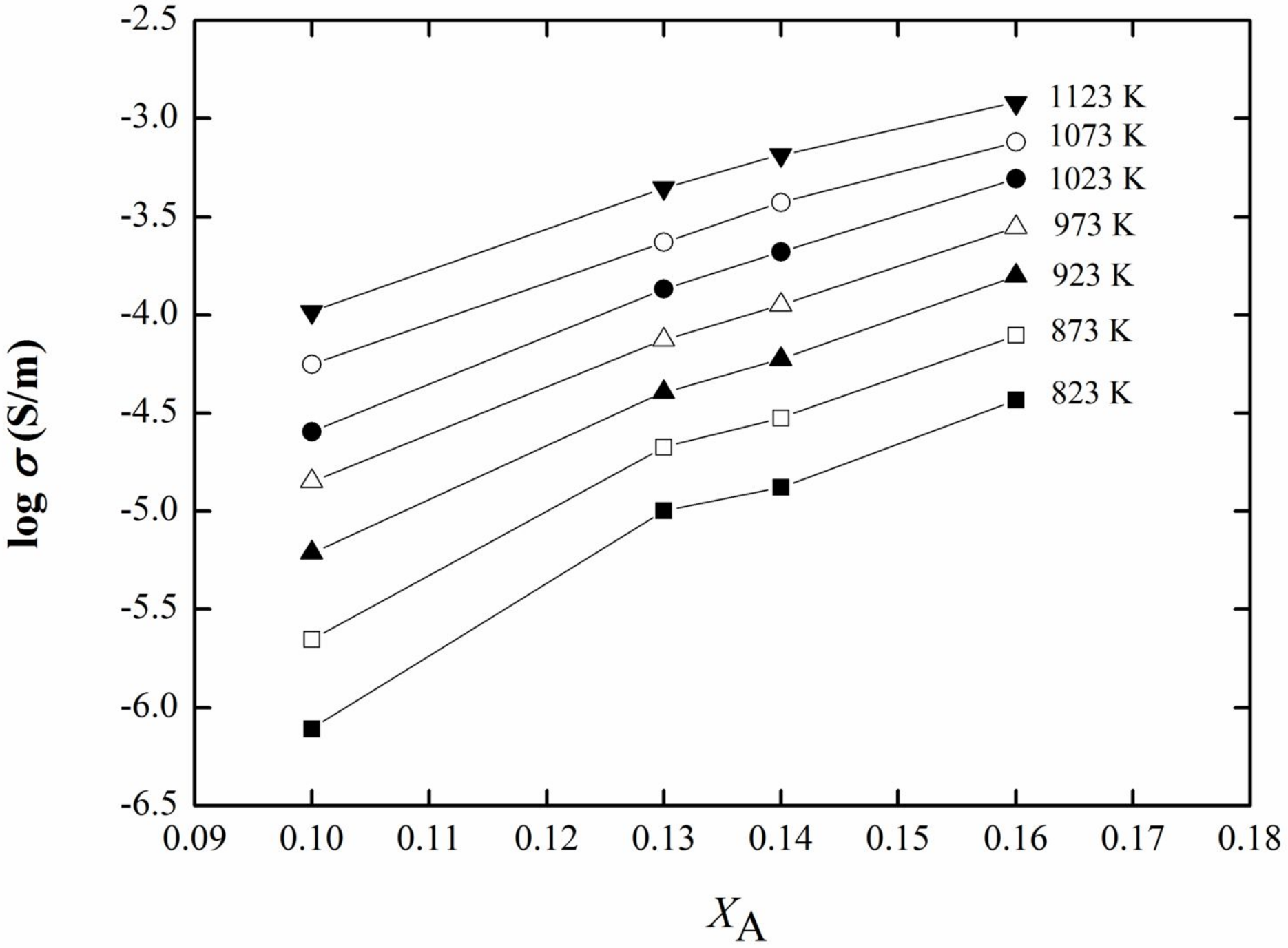
-2.5
-3.0
-3.5
-4.0
-4.5
-5.0
-5.5
-6.0
-6.5
0.09
0.10
0.11
0.12
0.13
0.14
0.15
0.16
0.17
0.18
log σ(S/m)
X_A
1123 K
1073 K
1023 K
973 K
923 K
873 K
823 K

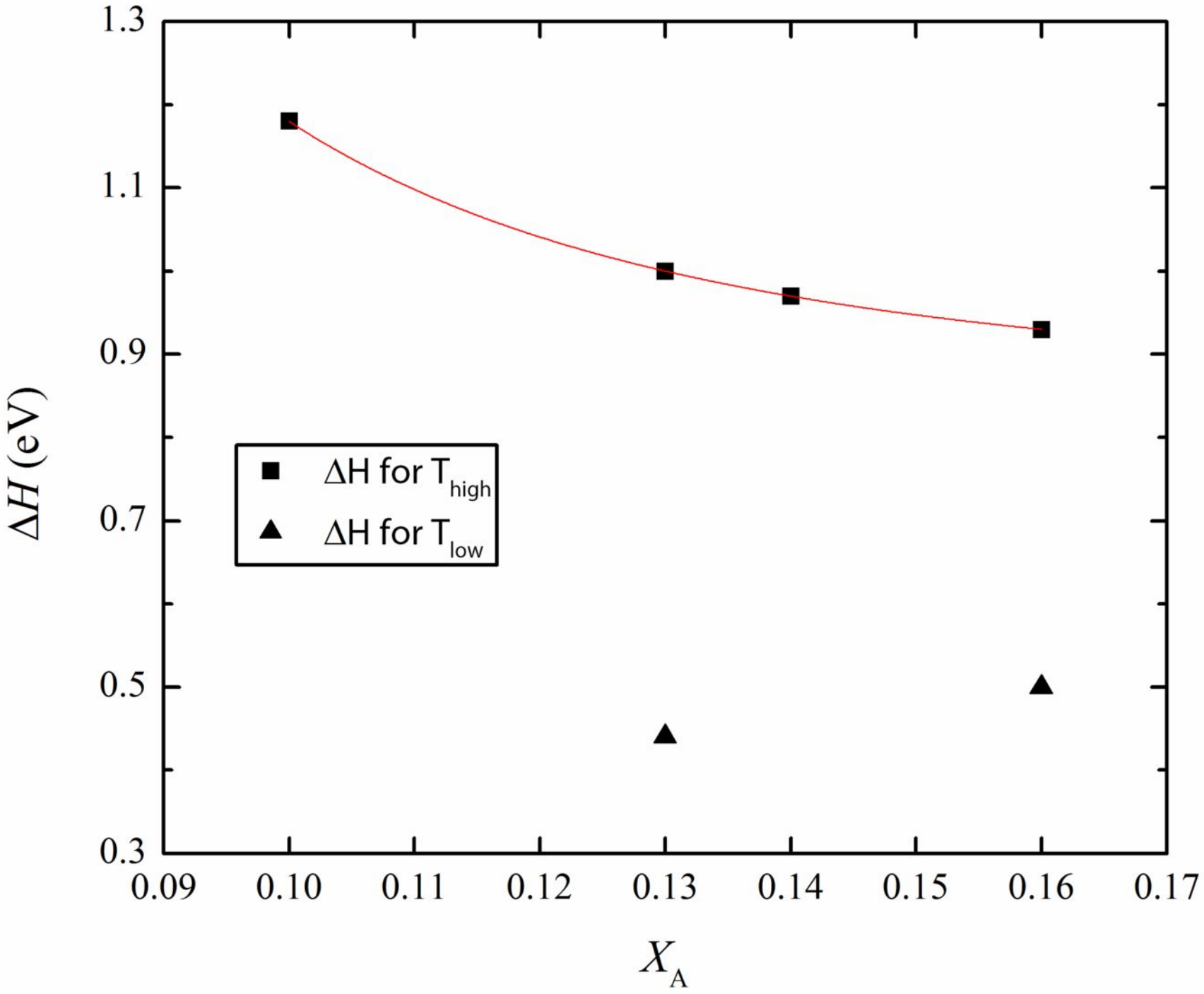
1.3
1.1
0.9
0.7
0.5
0.3
ΔH (eV)
0.09
0.10
0.11
0.12
0.13
0.14
0.15
0.16
0.17
X_A
ΔH for T_high
ΔH for T_low

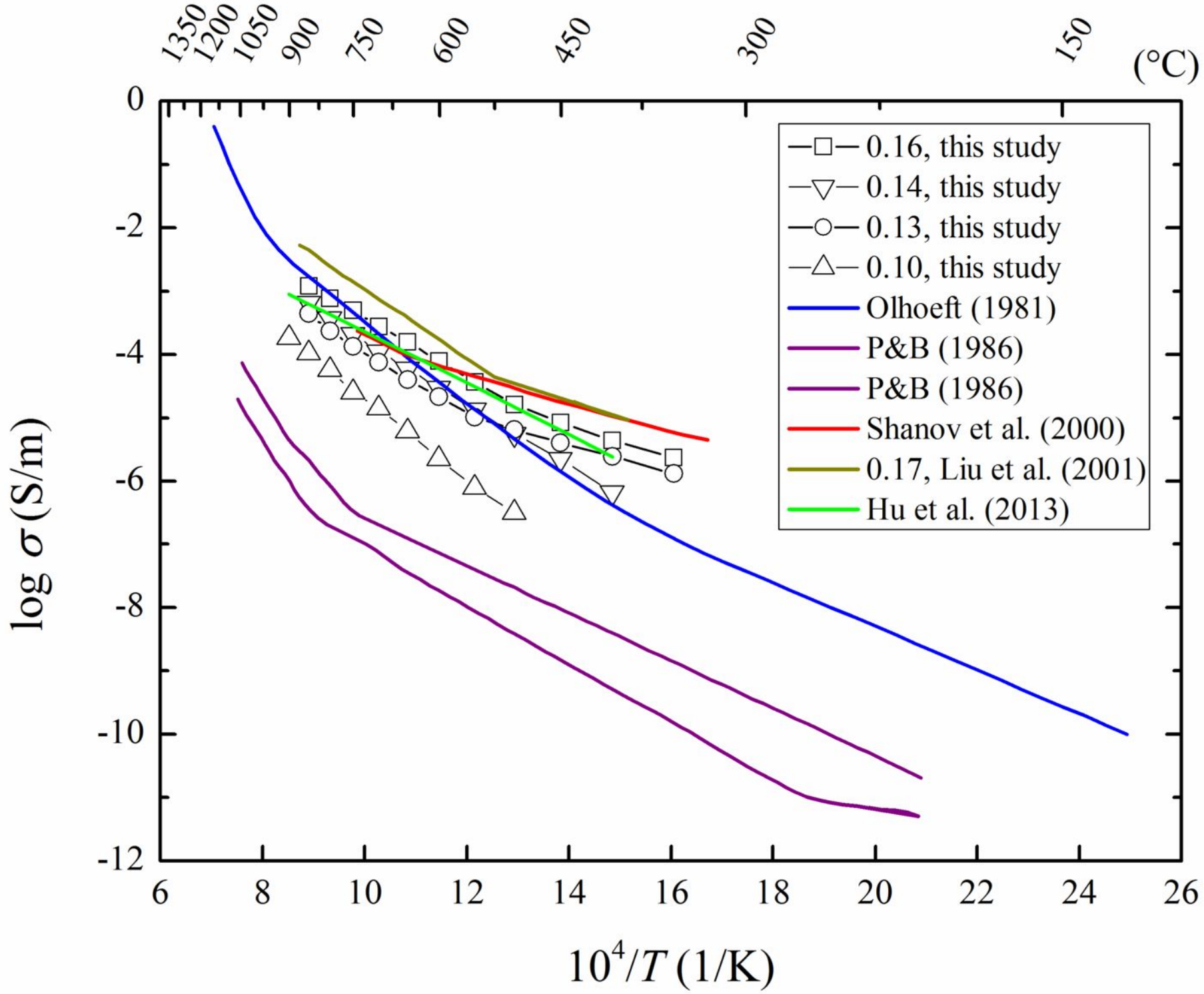
1350
1200
1050
900
750
600
450
300
150
(°C)
0
-2
-4
-6
-8
-10
-12
log σ (S/m)
6
8
10
12
14
16
18
20
22
24
26
10^4/T (1/K)
0.16, this study
0.14, this study
0.13, this study
0.10, this study
Olhoeft (1981)
P&B (1986)
P&B (1986)
Shanov et al. (2000)
0.17, Liu et al. (2001)
Hu et al. (2013)

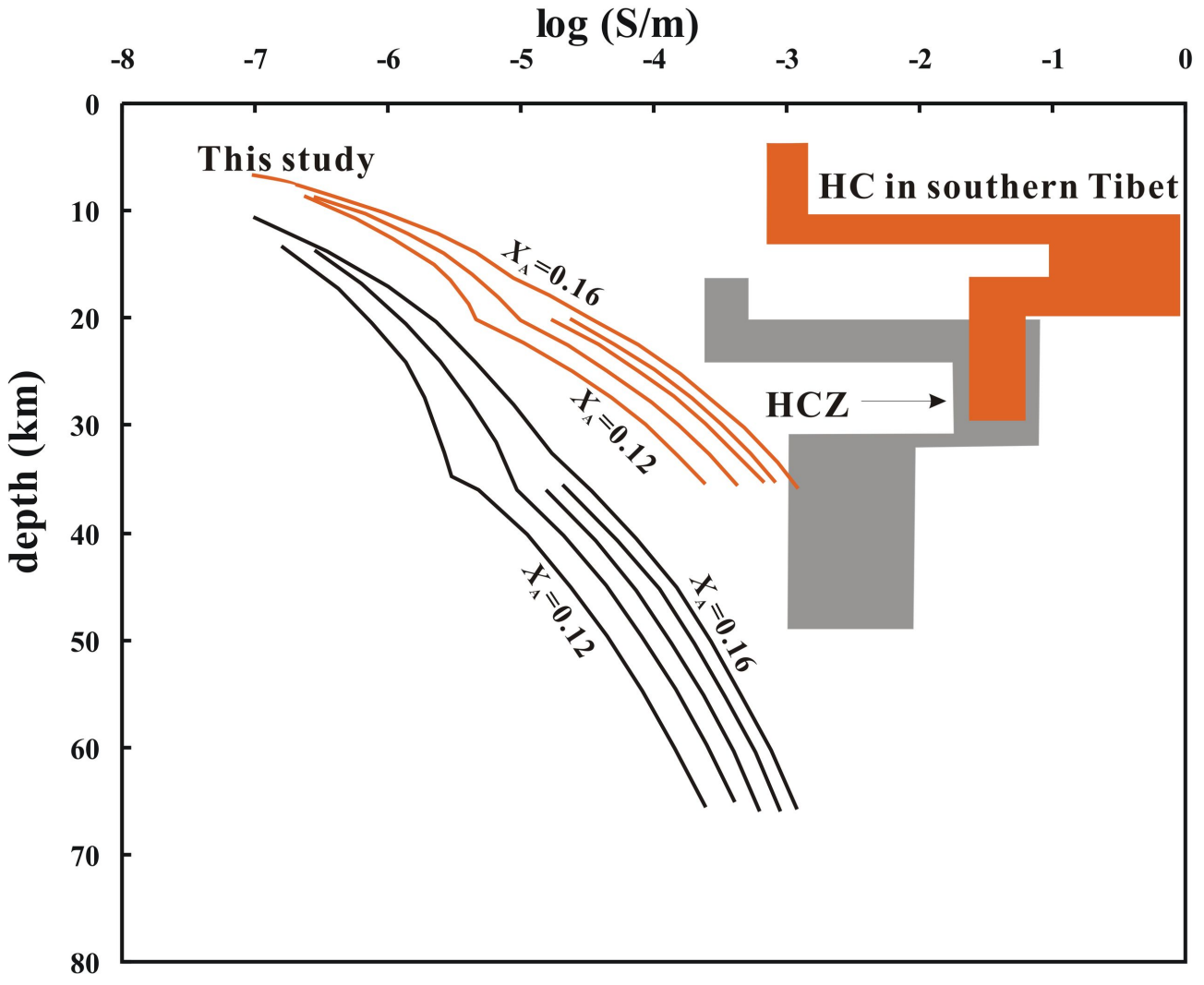
log (S/m)
-8
-7
-6
-5
-4
-3
-2
-1
0
depth (km)
0
10
20
30
40
50
60
70
80
This study
X_A=0.16
X_A=0.12
X_A=0.12
X_A=0.16
HC in southern Tibet
HCZ

Table 1. Major element content and mineral constituent of the granite samples analyzed by the X-ray fluorescence and point counting, respectively. X_A represents the weight percent ratio of $Na_2O + K_2O + CaO$ to SiO_2.

Oxide	HBP	XHS7	XHS8	SXW
SiO_2	68.26	72.22	74.69	79.29
TiO_2	0.29	0.02	0.02	0.06
Al_2O_3	16.35	14.92	13.04	12.05
Fe_2O_3	2.74	1.60	1.74	0.43
MnO	0.03	0.05	0.11	0
MgO	0.84	0	0.02	0.17
CaO	3.02	0.84	1.23	0.13
Na_2O	5.57	4.63	4.01	3.20
K_2O	2.41	4.44	4.68	4.97
P_2O_5	0.09	0.02	0.01	0.02
L.O.I	0.22	0.59	0.65	0.44
Total	99.82	99.33	100.20	100.76
X_A	0.16	0.14	0.13	0.10
feldspar	69%	64%	62%	58%
quartz	29%	34%	35%	37%
accessory minerals (biotite, amphibole, garnet,etc)	2%	2%	3%	5%

Note: The content of minerals in granites is volume percent; L.O.I, loss on ignition. All the values by X-ray fluorescence analysis are weight percent.

Table 2. Fitting parameters of electrical conductivity of granites obtained by Arrhenius formula.

Run no.	Sample no.	X_A	P (GPa)	T (K)	Log σ_0 (S/m)	ΔH (eV)
G1002	HBP	0.16	0.5	773-1123	1.24(3)	0.93(1)
				623-723	-1.63(15)	0.50(2)
G1203	XHS7	0.14	0.5	673-1123	1.18(6)	0.97(5)
G1308	XHS8	0.13	0.5-1.5	823-1123	1.03(13)	1.00(3)
				623-773	-2.31(4)	0.44(1)
G1406	SXW	0.10	0.5	773-1173	1.26(9)	1.18(2)

Talbe 3. The fitting parameters from the Equ. (3) and (4) for the electrical conductivity of granites

σ_0 (S/m)	ΔH_0 (eV)	α	β	γ
240(17)	0.85(3)	1.44(20)	3.46E-4(12)	-2.98(57)